

# Multi System Level Driving Scenarios Based Topology Optimization of Bracket Design for 2 DoF Vehicle Simulator

Bora Demirci<sup>1</sup>, Uğur Demir<sup>1</sup>, Gazi Akgün<sup>1</sup>, Alper Yıldırım<sup>1\*</sup> and Mustafa Caner Aküner<sup>1</sup>

0000-0001-9851-2829, 0000-0001-7557-3637, 0000-0002-8154-5883, 0000-0003-4814-5033, 0000-0001-8397-3454

<sup>1</sup> *Mechatronics Engineering Department, Faculty of Technology, Marmara University, Istanbul, 34854, Turkey*

## Abstract

This article presents a topology optimization of the motor mounting bracket in a 2-degree-of-freedom (2 DoF) vehicle simulator that is enhanced by the driving scenarios. Firstly, a 14 DoF passenger reference application model is determined in the Simulink environment. Then, common driving scenarios (Constant Radius, Double Lane Change, Fishhook, Increasing Steer, Sine with Dwell and Swept Sine) are run on 14 DoF vehicle models to test the dynamic performance of the vehicle. During the analysis, accelerations in the XYZ axes are logged, and the minimum and maximum acceleration values on each axis are grouped separately for each driving scenario. Next, the concept design of 2 DoF vehicle simulators is created. The obtained accelerations from the driving scenarios are then run on 2 DoF vehicle simulator in the Solidworks simulation environment, and stress and deformation on the 2 DoF vehicle simulator are analyzed. During this analysis, linear actuator and axis forces are calculated according to the reaction forces on the vehicle simulator. Under the determined axial forces, the brackets are subjected to topology optimization. The obtained generative design of the bracket is reshaped by post-processing for sustainable production. The shape-optimized bracket is run again on the 2 DoF vehicle simulator with the obtained acceleration values from the driving scenarios, and the study is completed by performing stress and deformation analysis.

Keywords: Generative design; Topology optimization; Dynamic analysis; Driving scenarios

## Research Article

<https://doi.org/10.30939/ijastech..1244113>

Received 30.01.2023  
Revised 10.06.2023  
Accepted 23.06.2023

\* Corresponding author  
Alper Yıldırım  
[yildirim.alper@marmara.edu.tr](mailto:yildirim.alper@marmara.edu.tr)  
Address: Mechatronics Engineering Department, Faculty of Technology, Marmara University, Istanbul, Turkey  
Tel: +902167773918

## 1. Introduction

Vehicle simulators are systems that are widely used in driver training or game platforms to create a digital twin of a real vehicle model. This allows the transfer of driving sensations such as maneuvering and acceleration to the driver, providing a realistic driving experience. These simulators can be used to measure the dynamic responses of the driver [1-5]. Linear actuators are typically used to connect the vehicle simulator to appropriate configuration, allowing the vehicle simulator to be considered as a parallel manipulator. An example of parallel manipulator known as Stewart platform is shown in Figure 1 [6].

Vehicle simulators or parallel manipulators primarily change the orientation of the platforms through the sequential movements of linear actuators [7]. In order to maintain the desired orientation of the platform, feedback such as displacement, velocity, and acceleration information is used to generate reference signals for the controller [8].

The real driving feeling on the vehicle simulator can be achieved

by transferring the reference accelerations of the linear actuators fed with the real driving information of the mobile platform on which the driver sits. The number and degree of freedom (DoF) of the actuators used can change depending on the mobile platform's connection points [9]. Parallel manipulators typically consist of base platform, a mobile platform, linear actuators and connection points between these components. As the mobile platform moves with the linear actuators, dynamic loads are generated between the mobile platform, the base platform and the actuator connection points. These dynamic loads can cause stress and deformation on the mounting brackets, this situation leads to preventing the natural operation of the system [10-11].

There are many studies in the literature on brackets. focusing on the optimization of their shape in sectors such as aviation and automotive, with the goal of reducing weight, improving fatigue life, and microstructures. These optimization studies often use topology optimization and heuristic approaches to address multi-objective requirements [12-14]. However, the studies typically focus on individual component. In this study, the brackets of a 2 degree-of-

freedom (2 DoF) vehicle simulator are considered in the context of enhanced topology optimization with driving scenarios at a multi-system level.



Fig. 1. Stewart Platform [6]

### 2. 2 DoF Vehicle Simulator

2 DoF vehicle simulator discussed in this study is shown in Figure 2. The system consists of vehicle body, linear actuators, driver seat, universal joint, mounting bracket, electronic control and

driver units, steer wheel, throttle, brake, and gear. The linear actuators are connected to the vehicle body and driver's seat with mounting brackets, and they actuate the driver's seat at the desired displacement, speed, and acceleration levels using reference signals from the electronic control unit. The dynamic model of general robotic system can be expressed in the form:

$$\tau = M(q)\ddot{q} + V(q, \dot{q}) + G(q) \tag{1}$$

$$\frac{d}{dt} \left( \frac{\partial K}{\partial \dot{x}} \right) - \frac{\partial K}{\partial x} + \frac{\partial U}{\partial x} + \sum_{i=1}^2 \zeta_i G_{i1} = \tag{2}$$

$$\frac{d}{dt} \left( \frac{\partial K}{\partial \dot{y}} \right) - \frac{\partial K}{\partial y} + \frac{\partial U}{\partial y} + \sum_{i=1}^2 \zeta_i G_{i2} = \tag{3}$$

$$\tau_1 = \frac{d}{dt} \left( \frac{\partial K}{\partial \dot{y}_1} \right) - \frac{\partial K}{\partial y_1} + \frac{\partial U}{\partial y_1} \sum_{i=1}^2 \zeta_i G_{i3} \tag{4}$$

$$\tau_2 = \frac{d}{dt} \left( \frac{\partial K}{\partial \dot{y}_2} \right) - \frac{\partial K}{\partial y_2} + \frac{\partial U}{\partial y_2} \sum_{i=1}^2 \zeta_i G_{i4} \tag{5}$$

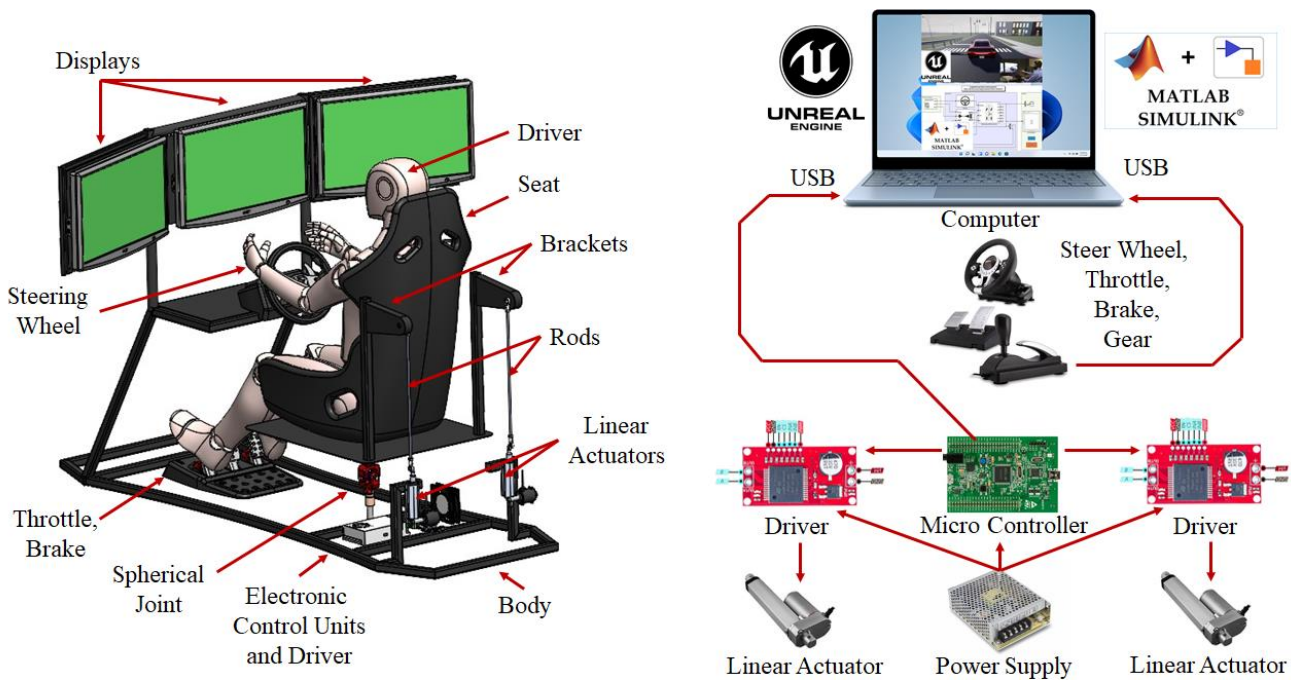


Fig. 2. 2 DoF Vehicle Simulator

The mathematical model with an integrated kinematic and dynamic for the 2 DoF vehicle simulator is represented between Equation (1) to (5). The Lagrangian formulation, instead of using the force and moments of the individual components, characterizes the behavior of a dynamic system in terms of work and energy stored in the system. This method allows for the systematic derivation of closed-form dynamical equations in any coordinate system. Here,  $M(q)$  is the positional mass matrix,  $V(q, \dot{q})$  is the vector of the nonlinear terms arising from the centripetal and Coriolis accelerations, and  $G(q)$  is the vector of the gravitational

terms.  $K$  is the total kinetic energy of the system,  $U$  is the total potential energy of the system,  $G_{ij}$  is element of the Jacobian matrix of constraint equation,  $\zeta_i$  Lagrange multiplier,  $\tau_i$  is the actuator force acting on the rods. [15-17].

These equations together describe the dynamics of a system with two degrees of freedom. The specific forms of the functions  $K$ ,  $U$ , and  $G_{i1}$ ,  $G_{i2}$ ,  $G_{i3}$ ,  $G_{i4}$  will depend on the system under consideration. Solving these equations will provide the equations of motion and describe the behavior of the system.

## 2.1 Driving Scenarios

In the literature, there are various test maneuvers used to analyze a vehicle's response to dynamic situations. These maneuvers are specially designed to evaluate how a component or subsystem affects overall vehicle handling, performance and stability. The widely used test procedures are preferred in this study. To evaluate and optimize the mounting brackets, the following driving scenarios are used: Constant Radius (CR) (SAE J266\_199601 and ISO 4138:2012), Double Lane Change (DLC) (ISO 3888-2), Fishhook (FH) (NHTSA standard), Increasing Steer (IS) (SAE J266), Sine with Dwell (SwD) (NHTSA standard), Swept Sine (SS) which are shown in Figure 3 [18-21].

Constant radius maneuver involves driving a vehicle at various speeds on a circular path with a fixed radius. It tests the vehicle's handling capabilities, self-steering behavior, and lateral stability.

The double lane change maneuver is designed to assess a vehicle's ability to quickly change lanes and avoid obstacles. The driver accelerates to a target speed, releases the throttle, steers to the left

lane, and then steers back to the right lane.

The fishhook maneuver is a test developed by the National Highway Traffic Safety Administration (NHTSA) to evaluate a vehicle's rollover resistance. It involves initiating a turn at a specific speed and steering angle, holding the steering angle for a duration, and then completing the maneuver.

The increasing steer maneuver is used to evaluate the lateral response of a vehicle. It involves gradually increasing the steering angle at a constant speed while the vehicle is traveling in a straight line.

In the sine with dwell maneuver, the vehicle is accelerated to a specific speed and then released without any steering or braking inputs. A sinusoidal steering input is then applied using a controller, with the frequency gradually increasing.

The swept sine maneuver tests the frequency response of a vehicle's steering inputs. The driver accelerates the vehicle to the target speed and applies a sinusoidal steering input, gradually increasing the frequency of the input.

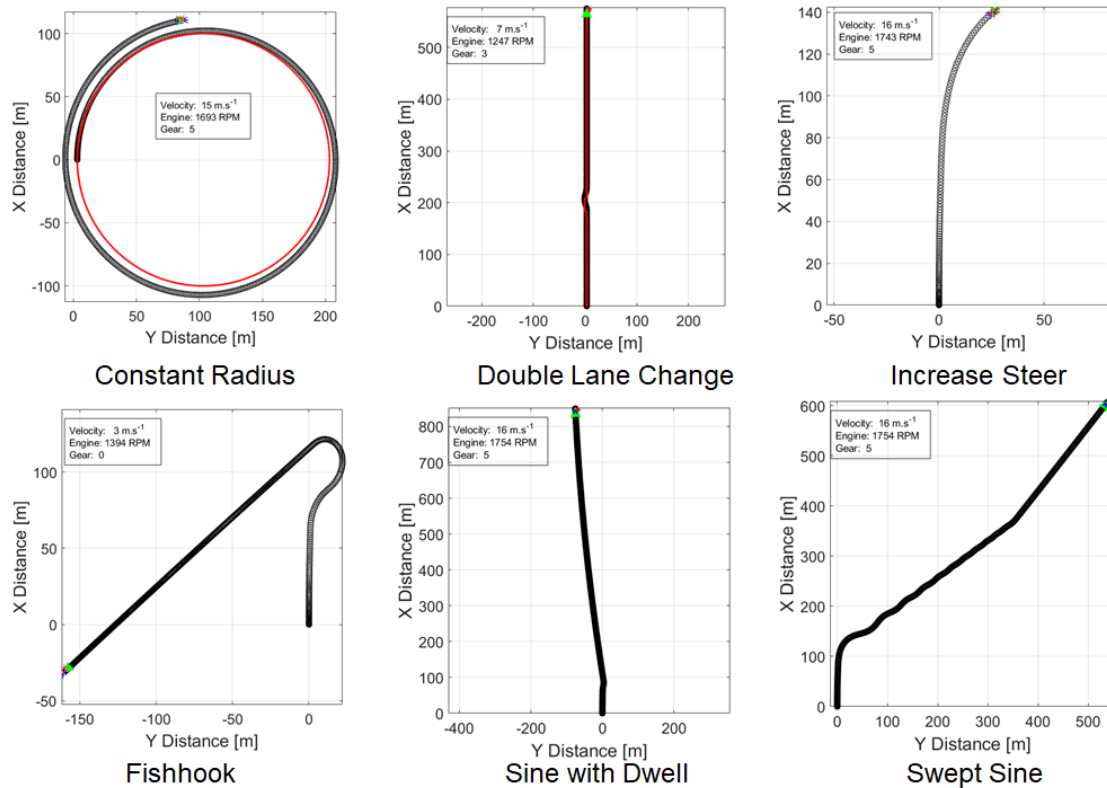


Fig. 3. Driving Scenarios

These maneuvers are designed to assess different aspects of a vehicle's dynamics, including stability, maneuverability, and response to steering inputs, providing valuable information for evaluating the vehicle's performance and safety.

## 2.2 Topology Optimization

Topology optimization is widely used for structural optimization to provide optimal material usage. For light-weighting, the

strength of the material is typically assessed through static and dynamic analysis.

$$E(\rho_e) = e^p E_0 \quad (6)$$

$$K(\rho) = \sum_{e=1}^N [\rho_{min} + (1 - \rho_{min}) \rho_e^p] K_e \quad (7)$$

$$C(\rho) = \sum_{e=1}^N \rho_e^p [u_e]^T [K_e] [u_e] \quad (8)$$

$$K(\rho)[u] = F \tag{9}$$

$$\frac{\partial c}{\partial \rho_e} = -p(\rho_e)^{p-1}[u_e]^T[K_e][u_e] \tag{10}$$

$$(K_i(\rho) - w^2M_i(\rho))u_i = F_i \tag{11}$$

$$\frac{\partial c}{\partial \rho_e} = 2F_i^T u_i \left( \frac{\partial F_i^T}{\partial \rho_e} u_i + F_i^T \frac{\partial u_i}{\partial \rho_e} \right) \tag{12}$$

Topology Optimization is typically implemented using Solid Isotropic Material with Penalization (SIMP) approach. This mathematical approach focuses on material density to meet the requirements [22-23]. The elasticity of the model is given in Equation (6). In this equation,  $\rho_e$  and  $E_0$  are material density and modulus of elasticity of the isotropic material. According to the SIMP method,

the hardness matrix is expressed as in Equation (7). where,  $K_e$  and  $N$  are the element stiffness matrix and number of elements in the design.

A common goal for topology optimization is to maximize stiffness in the model or to minimize coherence, which is the opposite of stiffness. Therefore, the optimization study analyzes the element density, which minimizes the global compatibility of the structure. The compatibility is given in Equation (8), where,  $u_e$  is the displacement vector of the element. The force is calculated using static and dynamic analysis, as given in Equation (9). The sensitivity is calculated as in Equation (10), and the damping effect is calculated as in Equation (11). In these equations,  $M$ ,  $w$  and  $i$  is the model mass matrix, angular frequency and the number of conditions in the optimization study. Finally, the sensitivity is re-arranged as in Equation (12) [24-26].

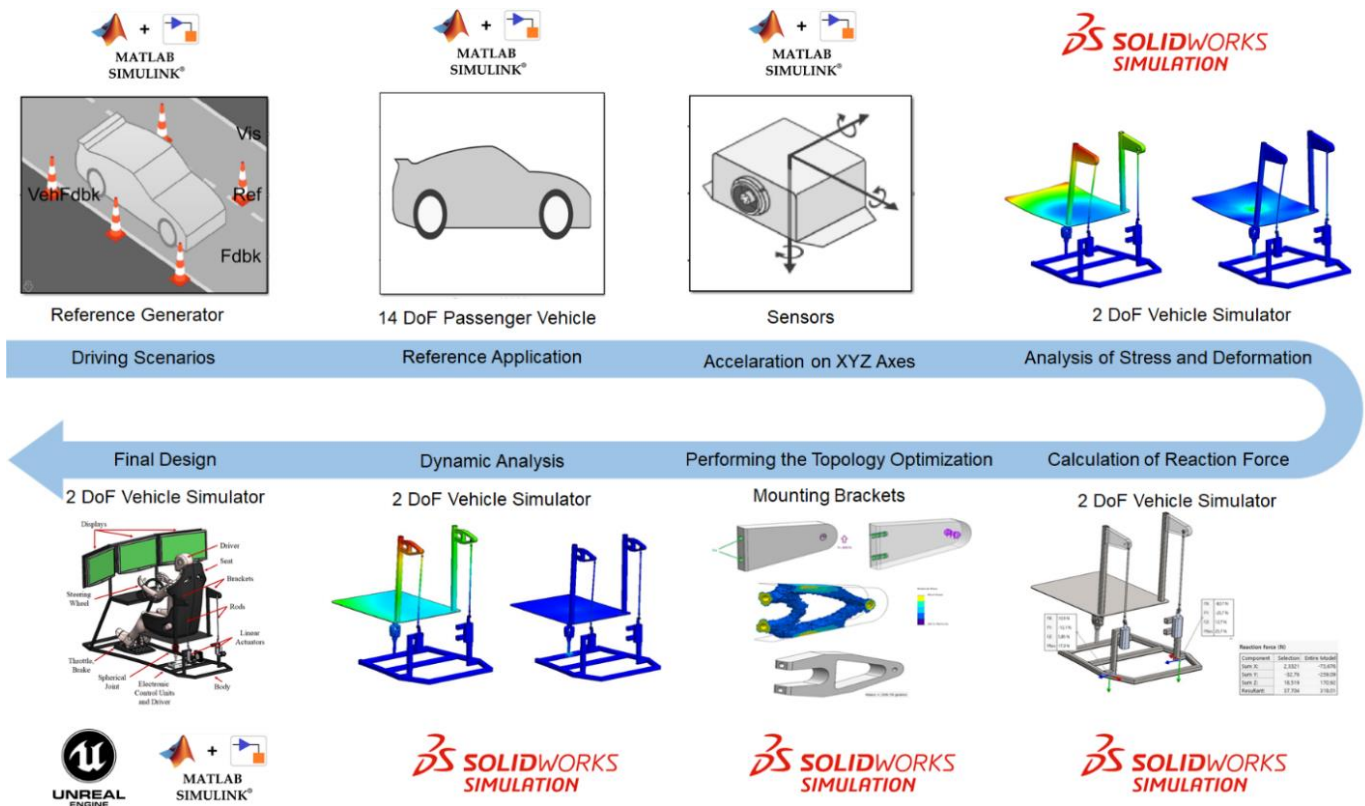


Fig. 4. Multi System Level Optimization Methodology

### 3. Materials and Method

In this study, the process steps for multi-system level optimization are shown in Figure 4. Firstly, the determined driving scenarios (CR, DLC, IS, FH, SwD and SS) are run on a reference application with 14 DoF passenger cars, and the acceleration values in the XYZ axes are analyzed. The stress and deformation analysis are carried out on the 2 DoF driving simulator according to the minimum and maximum values for the acceleration on XYZ axes obtained from driving scenarios. The resulting data is used to calculate the reaction force and determine the linear actuator force requirement. The topology optimization of the mounting bracket is

electronic control unit block using the actual feedback, and control signals are generated. These signals are used to control the steering and traction blocks of the vehicle block. Allowing it to track the reference signal. Table 1 provides the technical specifications of the passenger vehicle used in the reference application. The obtained acceleration on XYZ axes during the driving scenarios in the reference application are shown in Figure 6. As can be seen from Figure 6, the highest acceleration value occurred in the FH maneuver. The minimum and maximum accelerations on XYZ axes for all driving scenarios are given in Table 2

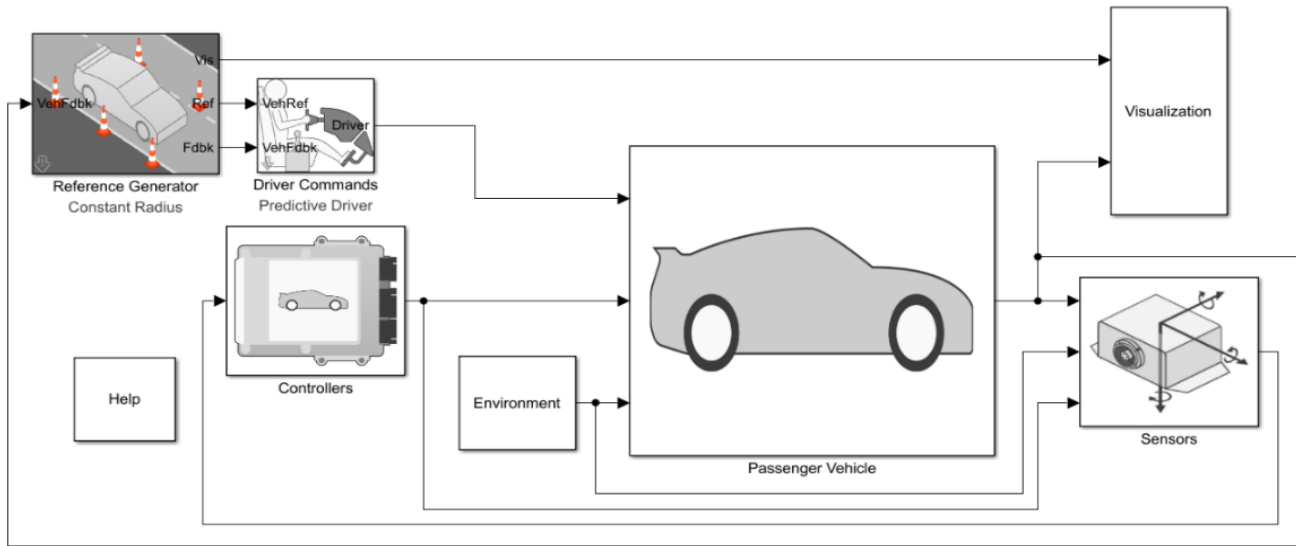


Fig. 5. Reference Application for 14 DoF Passenger Vehicle

Table 1. Technical Specifications of 14 DoF Passenger Vehicle

Body	Value	Unit	Transmission	Value	Unit
Mass	1600	kg	Drive Ratio	3.7	-
Wheel Base	3.075	m	Drive Efficiency	0.86	%
FrAxle Pos. from CG	1.515	m			
RrAxle Pos. from CG	1.504	m	Steering Front	Ackerman	
Height CG	0.134	m	Ratio	18	-
Frontal Area	2.11	m <sup>2</sup>	Range	3*pi	rad
Drag Coefficient	0.33				
Track Width	1.922	m	Driver		
Sprung Mass	1096.7	kg	Kp	400	-
			Ki	0.001	-
Engine			Pedal Filter Cons.	0.01	-
Max Power	100000	Watt			
Max Speed	7000	RPM	Suspension		
Stall Speed	200	RPM	Zeta	0.7071	-
			Wd	9.4248	-
Tire (205/60R15)			Stiffness	52451	N.m <sup>-1</sup>
Wheel Mass	11.433	kg	Damping	5565.2	N.s.m <sup>-1</sup>
Wheel Width	0.20905	m	Unsprung Mass Fr	21.0693	kg
Rim Radius	0.1914	m	Unsprung Mass Rr	21.0693	kg

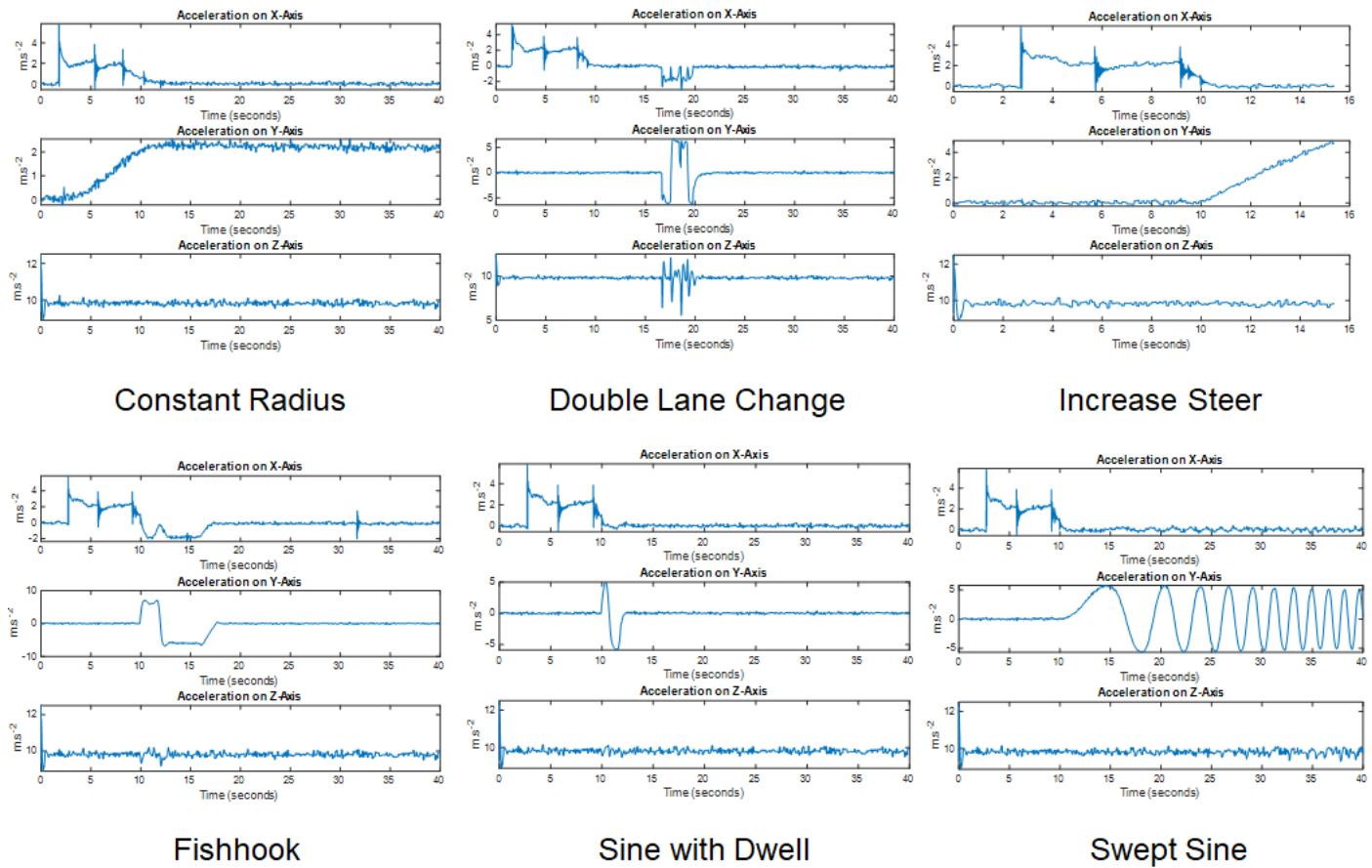


Fig. 6. Acceleration on XYZ Axes for Each Driving Scenarios

Table 2. Minimum and Maximum Accelerations on XYZ Axes

CR	Acceleration (m.s <sup>-2</sup> )		
Axis	X	Y	Z
X <sub>min</sub>	-0.48	0.51	9.6
X <sub>max</sub>	5.87	0.22	10.01
Y <sub>min</sub>	0.53	-0.23	10.25
Y <sub>max</sub>	0.27	2.54	9.68
Z <sub>min</sub>	-0.1	0.17	8.95
Z <sub>max</sub>	0.11	0.15	12.51

DLC	Acceleration (m.s <sup>-2</sup> )		
Axis	X	Y	Z
X <sub>min</sub>	-3.01	6.43	9.82
X <sub>max</sub>	5.48	0.08	9.78
Y <sub>min</sub>	-1.49	-6.12	11.95
Y <sub>max</sub>	-1.77	6.37	10.01
Z <sub>min</sub>	0.01	0.01	3.59
Z <sub>max</sub>	0.01	0.01	15.68

IS	Acceleration (m.s <sup>-2</sup> )		
Axis	X	Y	Z
X <sub>min</sub>	-0.43	0.1	9.72
X <sub>max</sub>	6.11	0.1	10.12
Y <sub>min</sub>	5.67	-0.12	9.87
Y <sub>max</sub>	0.07	4.89	9.81
Z <sub>min</sub>	0.01	0.01	8.87
Z <sub>max</sub>	0.01	0.01	12.5

FH	Acceleration (m.s <sup>-2</sup> )		
Axis	X	Y	Z
X <sub>min</sub>	-2.53	-6.07	9.89
X <sub>max</sub>	6.12	0.01	10.27
Y <sub>min</sub>	-0.27	-6.73	9.87
Y <sub>max</sub>	-2.01	6.82	9.54
Z <sub>min</sub>	0.01	0.01	8.91
Z <sub>max</sub>	0.01	0.01	12.5

SwD	Acceleration (m.s <sup>-2</sup> )		
Axis	X	Y	Z
X <sub>min</sub>	-0.48	0.01	9.81
X <sub>max</sub>	6.12	0.01	9.83
Y <sub>min</sub>	-0.12	-5.99	9.72
Y <sub>max</sub>	-0.17	5.12	9.57
Z <sub>min</sub>	0.01	0.01	8.85
Z <sub>max</sub>	0.01	0.01	12.5

SS	Acceleration (m.s <sup>-2</sup> )		
Axis	X	Y	Z
X <sub>min</sub>	-0.52	0.01	10.12
X <sub>max</sub>	6.17	0.01	9.68
Y <sub>min</sub>	-0.27	-5.93	9.93
Y <sub>max</sub>	0.29	5.96	10.01
Z <sub>min</sub>	0.01	0.01	8.89
Z <sub>max</sub>	0.01	0.01	12.5

#### 4. Results and Discussion

In this section, the obtained results and findings are discussed. The driving scenarios given in Figure 3 are run on the reference application of 14 DoF passenger cars shown in Figure 5. In the reference application, the driving scenarios are transformed into longitudinal and lateral reference signals by the reference generator and sent to the predictive driver block. The predictive driver block uses acceleration, deceleration, steering and gear information to control the vehicle block according to the dynamic response of the driver.

In the vehicle block, the received signals are evaluated by the electronic control unit block using the actual feedback, and control signals are generated. These signals are used to control the steering and traction blocks of the vehicle block. Allowing it to track the reference signal. Table 1 provides the technical specifications of the passenger vehicle used in the reference application.

The obtained acceleration on XYZ axes during the driving scenarios in the reference application are shown in Figure 6. As can be seen from Figure 6, the highest acceleration value occurred in the FH maneuver. The minimum and maximum accelerations on XYZ axes for all driving scenarios are given in Table 2.

Linear modal dynamic analysis was performed based on the maximum values of the accelerations obtained from 14 DoF vehicle models in the X, Y and Z axes over the section that gives the movement of the simulator chassis. Thus, the behavior of the simulator system under accelerations obtained from the relevant driving scenarios, that is, the results of stress and deformation, were examined. The simulator system has ST-37(S235JR) structural steel material, except for the bracket part. The material properties of ST-37 structural steel are shown in Table 3.

Table 3. ST-37 Structural Steel Material Mechanical Properties

Property	Value	Unit
Elastic Modulus	210000	N.mm <sup>-2</sup>
Poisson's Ratio	0.28	N.A <sup>-1</sup>
Shear Modulus	79000	N.mm <sup>-2</sup>
Mass Density	7800	kg.m <sup>-3</sup>
Tensile Strength	360	N.mm <sup>-2</sup>
Yield Strength	235	N.mm <sup>-2</sup>
Thermal Conductivity	14	W.(m.K) <sup>-1</sup>
Specific Heat	440	J.(kg.K) <sup>-1</sup>

All of the acceleration values in Table 2 were applied to the simulator system in modal dynamic analysis. For the modal dynamic analysis, the simulator system is assumed to be fixed from the base, and the fixation boundary condition is defined as in Figure 7.

In the modal dynamic analysis performed, the accelerations were applied as in Table 2 in the article. As an example, the Xmin values in the CR (Constant Radius) driving scenario are applied to the system together as acceleration in Figure 8.

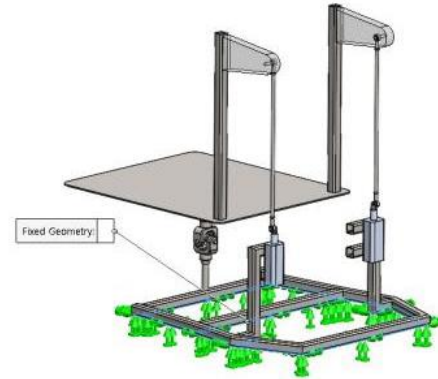


Fig. 7. Simulator Chassis Fixing

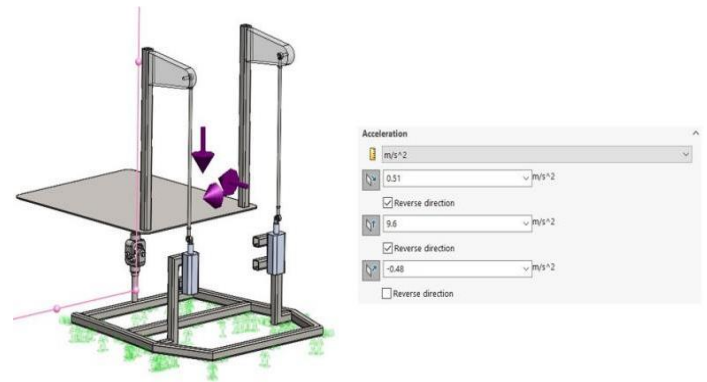
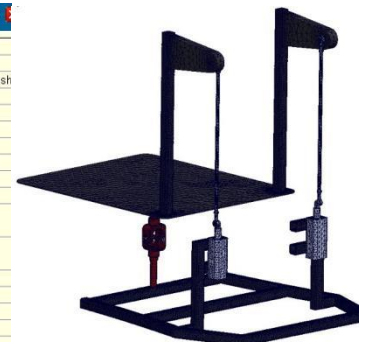


Fig. 8. Simulator Moving Structure CR Xmin Acceleration Values and Application

With the definition of the analysis boundary conditions, the mesh application process was carried out to solve the model. The mesh structure is applied in the same way in all modal dynamic analysis conditions and its details are shown in Figure 9.a. The maximum element size is 25 mm, the mini-mum element size is 5 mm. There are 357747 nodes, 187602 elements and high quality mesh is applied. Curvature-based tetrahedral mesh was applied. Figure 9.b shows the mesh structure in the system.

Mesh Details	
Study name	Xmin (Varsayilan-)
Mesh type	Solid Mesh
Meshes Used	Curvature-based mesh
Jacobian points for High quality mesh	16 points
Max Element Size	25 mm
Min Element Size	5 mm
Mesh quality	High
Total nodes	357747
Total elements	187602
Maximum Aspect Ratio	48.065
Percentage of elements with Aspect Ratio < 3	84.3
Percentage of elements with Aspect Ratio > 10	0.106
Percentage of distorted elements	0
Number of distorted elements	0
Remesh failed parts independently	Off
Time to complete mesh(hh:mm:ss)	00:00:25
Computer name	BDEMIRCI

a)



b)

Fig. 9. a) Mesh Details, b) Mesh Structure

After solving the modal dynamic analysis based on the relevant boundary conditions and mesh structure, Von-Mises stress and deformation results for each case are obtained and shown in Table 4.

Table 4. Modal Dynamic Analysis Stress and Deformation Results

CR	Stress (MPa)	Deformation (mm)	DLC	Stress (MPa)	Deformation (mm)	IS	Stress (MPa)	Deformation (mm)
X <sub>min</sub>	17.46	0.66	X <sub>min</sub>	129.18	3.31	X <sub>min</sub>	14.43	0.69
X <sub>max</sub>	74.92	0.53	X <sub>max</sub>	94.74	2.74	X <sub>max</sub>	77.49	0.55
Y <sub>min</sub>	15.6	0.74	Y <sub>min</sub>	112.01	3.49	Y <sub>min</sub>	73.03	0.55
Y <sub>max</sub>	43.11	1.47	Y <sub>max</sub>	113.62	3.23	Y <sub>max</sub>	84.41	2.49
Z <sub>min</sub>	13.12	0.61	Z <sub>min</sub>	5.31	0.25	Z <sub>min</sub>	13.09	0.62
Z <sub>max</sub>	18.57	0.81	Z <sub>max</sub>	23.14	1.09	Z <sub>max</sub>	18.45	0.87

FH	Stress (MPa)	Deformation (mm)	SwD	Stress (MPa)	Deformation (mm)	SS	Stress (MPa)	Deformation (mm)
X <sub>min</sub>	113.22	3.41	X <sub>min</sub>	15.52	0.71	X <sub>min</sub>	16.35	0.74
X <sub>max</sub>	77.25	0.57	X <sub>max</sub>	77.29	0.55	X <sub>max</sub>	77.95	0.54
Y <sub>min</sub>	120.24	3.53	Y <sub>min</sub>	89.24	1.19	Y <sub>min</sub>	106.26	3.19
Y <sub>max</sub>	123.17	3.41	Y <sub>max</sub>	88.63	2.59	Y <sub>max</sub>	102.99	2.94
Z <sub>min</sub>	13.15	0.62	Z <sub>min</sub>	13.06	0.61	Z <sub>min</sub>	13.12	0.62
Z <sub>max</sub>	18.45	0.87	Z <sub>max</sub>	18.45	0.87	Z <sub>max</sub>	18.45	0.87

Mesh convergence studies have been carried out in an exemplary manner based on the DLC (Double Lane Change) Xmin dynamic analysis scenario in which the highest stress value is seen in the article. Table 5. for the related mesh convergence study are given below.

It has been seen that the 25 mm 5 mm mesh application applied within the scope of the relevant study is generally sufficient. At the values close to these mesh sizes, it is seen that the stress values are close to each other in the analysis results, so the results converge.

Stress and deformation analysis are performed under the accelerations on 2 DoF vehicle simulators given in Table 2. The results of this analysis of stress and deformation are shown in Table 4. In the illustration in Table 4, displacements are shown with an exaggeration of 100 times. As a result of 36 modal dynamic analysis under the driving scenarios, the maximum stress is observed as 129.18 MPa in DLC. On the other hand, the maximum deformation is observed as 3.53 mm in FH.

In the case of the maximum stress and maximum deformation, the resultant force and reaction force are obtained as shown in Figure 10. The reaction force is observed as 319.01 N. Considering safety factor and standard product specification, the reaction force is determined as 400 N.

Table 5. Mesh Studies and Stress Results

Analyzes	Max Size(mm)	Min Size.(mm)	Stress(MPa)
Study-1	200	40	53,69
Study-2	100	20	65,71
Study-3	40	8	95,99
Study-4	35	7	111,53
Study-5	30	6	117,35
Study-6	29	5	129,2
Study-7	28	5	130,84
Study-8	27	5	128,31
Study-9	26	5	128,57
Study-10	25	5	129,18

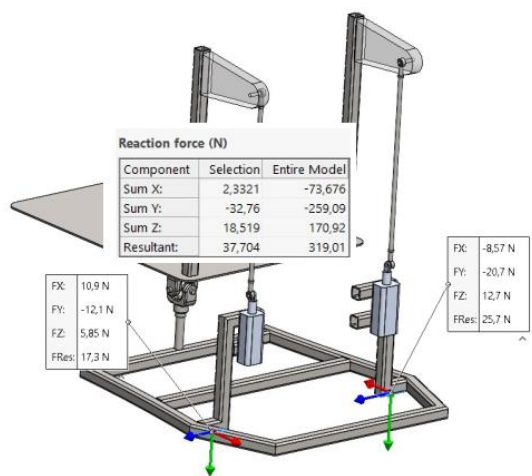


Fig. 10. The Resultant and Reaction Forces

To increase the system strength and lightness while reducing the deformation and stress values, topology optimization is used for the mounting brackets. In the topology optimization process, the mounting bracket is fixed through the bolt holes and a load of 400 N is applied vertically on the axis of the movement of the linear actuators to the screw shaft connection part to which the linear actuator is connected. The connection diagram and boundary conditions are shown in Figure 11. On the other hand, the mounting bracket is made of ABS PC, and its material properties are given in Table 5.

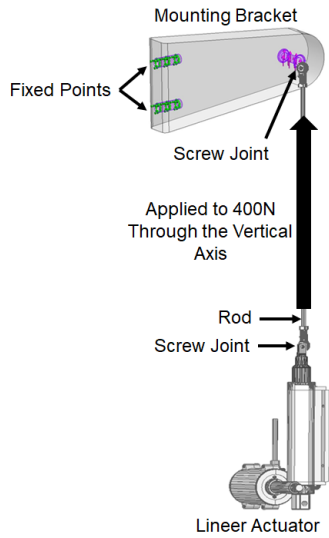


Fig. 11. The Boundary Condition and Connection Points Between the Linear Actuator and Mounting Bracket

Table 6. Minimum and Maximum Accelerations on XYZ Axes

Property	Value	Unit
Elastic Modulus	241	N.mm <sup>-2</sup>
Poisson's Ratio	0.3897	N.A <sup>-1</sup>
Shear Modulus	862.2	N.mm <sup>-2</sup>
Mass Density	1070	kg.m <sup>-3</sup>
Tensile Strength	40	N.mm <sup>-2</sup>
Thermal Conductivity	0.2618	W.(m.K) <sup>-1</sup>
Specific Heat	1900	J.(kg.K) <sup>-1</sup>

In this study, the objective function for the topology optimization of the mounting bracket is weight reduction with a maximum stress constraint of 20 MPa. The resulting optimized design is shown in Figure 12. This design is then processed to generate the final generative design, as shown in Figure 13.

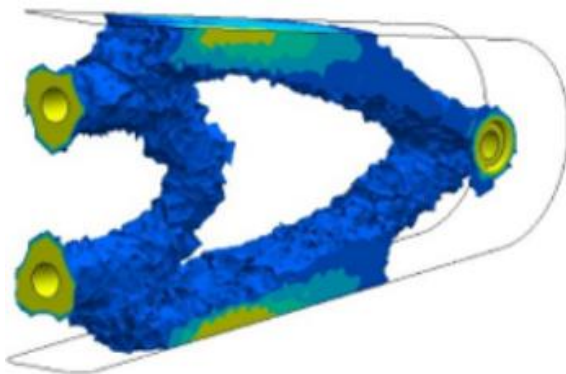


Fig. 12. The Optimization Results for the Mounting Bracket

At initial stage, the mounting bracket shown in Figure 11 has a mass with 0.47717 kg. After the topology optimization, the mass of the mounting bracket shown in Figure 10 is reduced to 0.20819 kg. This

result shows that a weight reduction of 56.4% has been achieved.

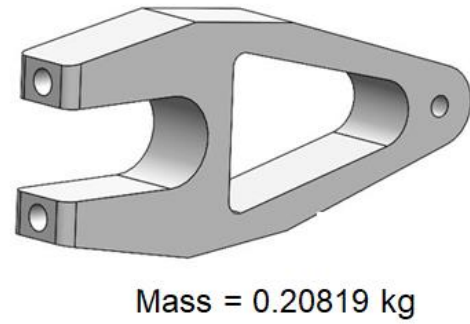


Fig. 13. The Generative Design for the Mounting Bracket

The obtained generative design is subjected to dynamic analysis to evaluate its stress and deformation performance. In the case of DLC scenario, the von-mises stress is reduced from 129.18 MPa to 126.42 MPa and the maximum deformation is reduced from 3.31 mm to 2.98 mm. These results show that the improvements in the mounting bracket are 2.2% for stress and 10% for the deformation. Furthermore, a decrease of 70.6% from 71.1% is observed in the mass participation rate in the X-axis at the same frequency mode number (30 modes), indication a reduction in the moment of inertia. The results of the dynamic analysis for the generative design of the mounting bracket are shown in Figure 14.

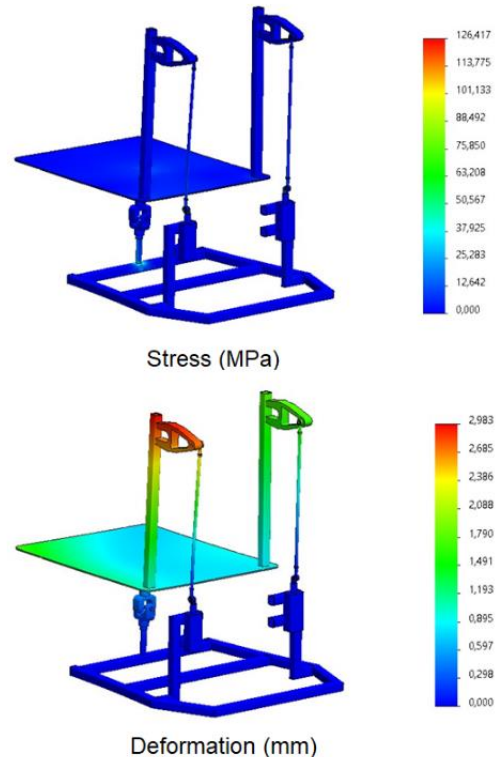


Fig. 14. The Generative Design Dynamic Analysis Under DLC Scenario

### 5. Conclusion

In this study, multi-system level topology optimization based on driving scenarios is studied for 2 DoF vehicle simulator brackets. First of all, the commonly used driving scenarios for analyzing the

dynamic performance of a vehicle and its components are determined as CR, DLC, IS, FH, SwD and SS. These scenarios are then run on a passenger vehicle with 14 DoF. During the driving scenarios, the acceleration information on the XYZ axes is logged. Using the obtained maximum and minimum acceleration values, the concept 2 DoF vehicle simulator with 36 different configurations is analyzed in terms of stress and deformation. The results show that the maximum stress is in the DLC scenario (129.18 MPa) and the maximum deformation is in the FH scenario (3.53 mm).

According to the maximum stress, the resultant and reaction forces in the DLC scenarios are analyzed. In the DLC scenario, the reaction force is 319.01 N, so the linear actuator providing a reaction force of 400 N is chosen as a standard product. Then, the objective function for the topology optimization is then determined as mass minimization with the maximum stress of 20 MPa as the design constraint. The generative bracket design as shown in Figure 14 as a result of topology optimization is obtained under these conditions, then it is evaluated in comparison with the initial bracket as shown in Figure 12. The results show that the weight reduction of 56.4% is achieved. Additionally, stress and deformation analysis are performed on the generative bracket design under the DLC scenario. In the obtained findings, an improvement of 2.2% for maximum stress and 10% for deformation are achieved. Moreover, the moment of inertia is reduced with a 0.5% improvement in the mass participation rate. According to the obtained results, it is observed that topology optimization can be improved with multi-system level based on driving scenarios for determining and evaluating the objective function and design constraints of a vehicle component.

### Acknowledgment

This work was supported by Marmara University Scientific Research Projects Commission (Project No: FYL- 2022-10537).

### Nomenclature

$\tau_i$	: Actuator force acting on the rods (N)
$M(q)$	: Positional mass matrix (kg)
$V(q, \dot{q})$	: Vector of the nonlinear terms arising from the centripetal and Coriolis accelerations
$G(q)$	: Vector of the gravitational
$K$	: Total kinetic energy of the system (Joule)
$U$	: Total kinetic energy of the system (Joule)
$G_{ij}$	: Element of the Jacobian matrix of constraint
$\zeta_i$	: Lagrange multiplier
<i>DLC</i>	: Double Lane Change
<i>CR</i>	: Constant Radius
<i>IS</i>	: Increase Steer
<i>FH</i>	: Fishhook
<i>SS</i>	: Swept Sine
<i>SwD</i>	: Sine with Dwell
<i>Xmin</i>	: Minimum value on x-axis
<i>Xmax</i>	: Maximum value on x-axis
<i>Ymin</i>	: Minimum value on y-axis
<i>Ymax</i>	: Maximum value on y-axis

$Z_{min}$	: Minimum value on z-axis
$Z_{max}$	: Maximum value on z-axis
$\rho_e$	: Material density
$E_0$	: Modulus of elasticity
$K_e$	: Stiffness matrix and
$N$	: Number of elements
$u_e$	: Displacement Vector
$M$	: Mass matrix
$w$	: Angular frequency
$i$	: Number of conditions
$F$	: Applied Force Vector
$C$	: SIMP Optimization Variable

### Conflict of Interest Statement

The authors declare that there is no conflict of interest in the study.

### CRedit Author Statement

**Mustafa Caner Aküner:** Supervision,

**Uğur Demir:** Supervision, Methodology, Project administration, Validation

**Gazi Akgün:** Supervision including mentorship, Validation

**Alper Yıldırım:** Conceptualization, Writing-original draft,

**Bora Demirci:** Conceptualization, Data curation, Formal analysis

### References

- [1] Bang KH. Development of dynamics modeling in the vehicle simulator for road safety analysis. SICE Annual Conference 2007; 649-653. doi: 10.1109/SICE.2007.4421062.
- [2] Reddy GN. An EV-simulator for Electric Vehicle Education. International Conference on Engineering Education (ICEED) 2009; 131-137. doi: 10.1109/ICEED.2009.5490597.
- [3] Peng J, Zhenjun S. Improvement of driving simulator for real-time vehicle dynamic collision simulation. 2nd IEEE International Conference on Computer Science and Information Technology 2009; 590-593. doi: 10.1109/ICCSIT.2009.5234631.
- [4] Zhao Y, et al. Integrated Traffic-Driving-Networking Simulator: A Unique R&D Tool for Connected Vehicles. International Conference on Connected Vehicles and Expo (ICCV) 2012; 203-204. doi: 10.1109/ICCV.2012.45.
- [5] Weiss E, Gerdes JC. High Speed Emulation in a Vehicle-in-the-Loop Driving Simulator. IEEE Transactions on Intelligent Vehicles 2022; doi: 10.1109/TIV.2022.3162549.
- [6] Jianjun H, Hehong G, Zhelong W. Solving the forward kinematics problem of six-DOF Stewart platform using multi-task Gaussian process. Proceedings of the Institution of Mechanical Engineers Part C Journal of Mechanical Engineering Science 2013; 227: 161-169. doi: 10.1177/0954406212444508.
- [7] Kim KD, Kim MS, Moon YG, Lee MC. Application of Vehicle Driving simulator Using New Washout Algorithm and Robust Control. SICE-ICASE International Joint Conference 2006; 2121-2126. doi: 10.1109/SICE.2006.315563.
- [8] Kulothungan S, Anirudh RV, Sivashankar K, Dash AK. Design and

- Development of a Vehicle Dynamics Model for a Drive Simulator. 3rd International Conference on Communication and Electronics Systems (ICCES) 2018; 153-156. doi: 10.1109/CESYS.2018.8723987.
- [9] Shuxian X, Linxuan Z. Simulating driving feel for virtual driving simulator based on semi-physical simulation. 34th Chinese Control Conference (CCC) 2015; 8882-8887. doi: 10.1109/ChiCC.2015.7261043.
- [10] Patel Y, George P. Parallel Manipulators Applications—A Survey. *Modern Mechanical Engineering* 2012; 2(3):57-64. doi: 10.4236/mme.2012.23008.
- [11] Hernández A, Urizar M, Macho E, Petuya V. Parallel Manipulators: Practical Applications and Kinematic Design Criteria. *Towards the Modular Reconfigurable Robots. Mechanisms, Transmissions and Applications. Mechanisms and Machine Science* 2017; 52. doi:10.1007/978-3-319-60702-3\_14
- [12] Gökdağ İ, Acar E. Application of a modular topology optimization framework to an aerospace bracket design. *Materials Testing* 2022; 64(7): 1090-1102. doi: 10.1515/mt-2021-2148
- [13] Arıci BB, Armağan A, Yılmaz M, Serap G, Yücel SC. Microstructural and mechanical properties of friction and MIAB welded carbon steel tubes and forging bracket joints. *Materials Testing* 2018; 60(3): 273-282. doi:10.3139/120.111144
- [14] Korkmaz FF, Subran M, Yıldız AR. Optimal design of aerospace structures using recent meta-heuristic algorithms. *Materials Testing* 2021; 63(11): 1025-1031. doi:10.1515/mt-2021-0024
- [15] Liu XJ, Wang QM, Wang J. Kinematics, dynamics and dimensional synthesis of a novel 2-DoF translational manipulator. *J. Intell. Robot. Syst.* 2005; 41(4): 205–224. doi: 10.1007/s10846-005-3507-z.
- [16] Zhao TS, Huang Z. A Novel Three-DOF Translational Platform. *Mechanism and its Kinematics* 2000; 517–522. doi: 10.1115/DETC2000/MECH-14101.
- [17] Ganesh SS, Rao ABK. Kinematic and Dynamic Optimization of a 2-DOF Parallel Kinematic Mechanism. *Procedia Comput. Sci.* 2018; 133: 576–584. doi:10.1016/j.procs.2018.07.086.
- [18] Karlsson A. Test Procedures and Evaluation Tools for Passenger Vehicle Dynamics. *Computer Science*. 2014.
- [19] SAE International. J266: Steady-State Directional Control Test Procedures for Passenger Cars and Light Trucks 2018;4970(724)
- [20] ISO 3833:1977 - Road vehicles — Types — Terms and definitions. 2022.
- [21] Bosch Automotive Handbook, 9th Edition. 2014. doi: 10.4271/0768081521.
- [22] Rozvany GIN, Zhou M, Birker T. Generalized shape optimization without homogenization. *Struct. Optim.* 1992; 4(3-4): 250–252. doi: 10.1007/bf01742754.
- [23] Bendsoe P, Kikuchi N. Generating optimal topologies in structural design using a homogenization method. *Comput. Methods Appl. Mech. Eng.* 1988; 71(2): 197–224. doi: 10.1016/0045-7825(88)90086-2.
- [24] Isik M, et al. Topology Optimization and Manufacturing of Engine Bracket using Electron Beam Melting. *J. Addit. Manuf. Technol.* 2021.
- [25] Shi G, Guan C, Quan D, Wu D, Tang L, Gao T. An aerospace bracket designed by thermo-elastic topology optimization and manufactured by additive manufacturing. *Chinese J. Aeronaut.* 2020;33(4): 1252–1259. doi: 10.1016/j.cja.2019.09.006.
- [26] Chen Y, et al. Topology optimization design and experimental research of a 3d-printed metal aerospace bracket considering fatigue performance. *Appl. Sci.* 2021; 11(15). doi: 10.3390/app11156671.